

Secure Cell-Free Massive MIMO ISAC Systems: Joint AP Selection and Power Allocation Against Eavesdropping

Ruiguang Wang*, Takumi Takahashi*, and Hideki Ochiai*

* Graduate School of Engineering, The University of Osaka, 2-1 Yamada-oka, Suita, 565-0871, Japan

Email: *{r-wang@wcs., takahashi@, ochiai@}comm.eng.osaka-u.ac.jp,

Abstract—This paper investigates a cell-free massive multiple-input-multiple-output (CF-mMIMO) integrated sensing and communication (ISAC) system that addresses the critical challenge of information leakage to potential eavesdroppers located within sensing zones. A novel access point (AP) selection strategy is proposed, which partitions the distributed APs into two functional groups: communication APs (C-APs), dedicated exclusively to data transmission, and sensing APs (S-APs), responsible for target detection and eavesdropper suppression. Closed-form expressions for the achievable communication rate, eavesdropping rate, and mainlobe-to-average-sidelobe ratio (MASR) are derived to evaluate system performance. Two complementary optimization problems are formulated using the successive convex approximation (SCA): (i) maximizing user rates under security constraints and (ii) minimizing eavesdropping rates while satisfying quality of service (QoS) requirements. The proposed joint optimization framework determines the optimal AP operational modes and power allocation across communication and sensing links. Extensive numerical results validate the theoretical analysis and demonstrate significant performance gains, revealing inherent trade-offs among communication efficiency, sensing accuracy, and security. These insights offer practical guidelines for designing secure CF-mMIMO ISAC systems.

Index Terms—Integrated sensing and communication, physical layer security, power allocation.

I. INTRODUCTION

Future 6G networks must deliver ultra-high communication rates while enabling precise environmental sensing for applications ranging from autonomous driving to digital twins [1], [2]. Meanwhile, cell-free massive multiple-input-multiple-output (CF-mMIMO) provides superior spectral efficiency and coverage uniformity [3]. The synergy between these technologies is compelling, as CF-mMIMO's distributed antenna arrays can simultaneously support high-throughput communication and high-precision radar sensing [4].

However, CF-mMIMO-based integrated sensing and communication (ISAC) systems face critical security vulnerabilities. The unified waveform design allows sensing targets to potentially intercept confidential information [5]. Moreover, the reduced number of antennas per access point (AP) weakens beamforming accuracy, which has conventionally served as a safeguard against eavesdropping. While security improvements in traditional ISAC systems have been thoroughly investigated [6], the security of CF-mMIMO ISAC is still largely unexamined.

An optimal transmission strategy was proposed in [7] that utilizes artificial noise to impair eavesdropper reception while

minimizing the constrained Cramér-Rao bound via semidefinite relaxation, thus achieving a balance among sensing accuracy, communication quality, and security. The study in [8] focuses on optimizing joint transmit beamforming among multiple ISAC transmitters to enhance legitimate detection probability. It ensures communication quality and reduces the risks of data eavesdropping and sensing information interception by employing semidefinite relaxation, which has demonstrated global optimality. Furthermore, [9] introduces a joint optimization framework utilizing minorization-maximization and semidefinite programming to develop transmit beamforming and fronthaul compression, aimed at improving sensing performance while adhering to secure communication and capacity constraints. Unified waveforms, however, pose a risk of information leakage to sensing targets during sensing operations.

This paper investigates a CF-mMIMO ISAC system wherein distributed APs simultaneously serve multiple user equipment (UE) devices and sensing multiple zones. We propose a novel joint AP selection and power allocation method that assigns each AP to either communication or sensing [10], thereby reducing information leakage. The primary contributions include: (i) the derivation of closed-form expressions for the communication rate, eavesdropping rate, and mainlobe-to-average-sidelobe ratio (MASR); (ii) the formulation of optimization problems aimed at maximizing communication rates or minimizing eavesdropping rates under sensing and power constraints; and (iii) validation of the proposed framework through comprehensive numerical results.

Notation: Bold lowercase letters and uppercase letters denote vectors and matrices, respectively. The superscript $(\cdot)^\dagger$ represents the conjugate transpose and \mathbf{I}_N denotes the $N \times N$ identity matrix. The statistical expectation operator is denoted by $\mathbb{E}[\cdot]$ and $\mathcal{CN}(\boldsymbol{\mu}, \boldsymbol{\sigma}^2)$ represents a complex jointly Gaussian distribution with mean vector $\boldsymbol{\mu}$ and covariance matrix $\boldsymbol{\sigma}^2$.

II. SYSTEM MODEL

Consider a CF-mMIMO ISAC system illustrated in Fig. 1, where M APs simultaneously serve K UEs while sensing L zones. Each AP is equipped with N antennas arranged in a uniform linear array (ULA), whereas both UEs and targets, which are regarded as potential eavesdroppers, located within the sensing zones are equipped with a single antenna. To enhance security, we adopt an AP selection strategy [10] that

assigns AP as either a communication AP (C-AP) or a sensing AP (S-AP), thereby preventing information leakage through separated signal transmission.

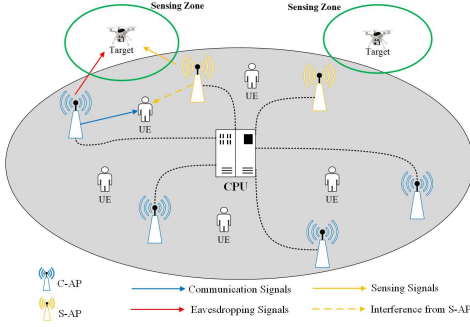


Fig. 1. Illustration of the CF-mMIMO ISAC system.

A. Channel Model

We assume quasi-static block fading channels that remain constant over coherence intervals of τ symbols, with τ_t symbols allocated for training. The channel between AP m and UE k is expressed as $\mathbf{g}_{mk} = \sqrt{\beta_{mk}} \mathbf{h}_{mk}$, where β_{mk} denotes the large-scale fading and $\mathbf{h}_{mk} \sim \mathcal{CN}(\mathbf{0}, \mathbf{I}_N)$ represents the small-scale fading. Using linear minimum mean square error (LMMSE) estimation [11], the channel estimate is distributed as $\hat{\mathbf{g}}_{mk} \sim \mathcal{CN}(\mathbf{0}, \gamma_{mk} \mathbf{I}_N)$, where $\gamma_{mk} \triangleq \frac{\tau_t \rho_t \beta_{mk}^2}{\tau_t \rho_t \beta_{mk} + 1}$ and ρ_t denotes the pilot transmit power.

For the sensing channel model, the APs are assumed to possess prior knowledge of the sensing zones. The direction from AP m to sensing zone l is denoted by θ_{ml} , representing the angle of departure (AoD) determined by their relative positions. The sensing channel between AP m and sensing zone l is modeled as $\mathbf{g}_{ml} = \sqrt{\zeta_{ml}} \mathbf{a}_N(\theta_{ml})$, where ζ_{ml} represents the distance-dependent path loss and $\mathbf{a}_N(\theta_{ml}) \in \mathbb{C}^{N \times 1}$ is the array response vector whose n -th element is expressed as

$$[\mathbf{a}_N(\theta_{ml})]_n = \exp \left[j \frac{2\pi d}{\lambda} (n-1) \sin(\theta_{ml}) \right], \quad (1)$$

with d and λ representing the antenna spacing and carrier wavelength, respectively.

B. Signal Structure and Transmission

Let \mathbf{x}_m^c and \mathbf{x}_m^s denote the communication and sensing signals, respectively. For later convenience, the transmitted signal at the m -th AP is defined as

$$\mathbf{x}_m \triangleq \sqrt{a_m} \mathbf{x}_m^c + \sqrt{1-a_m} \mathbf{x}_m^s, \quad (2)$$

where $a_m \in \{0, 1\}$ is a binary variable indicating the operational mode of the m -th AP. During the downlink transmission phase, C-APs transmit data signals to UEs employing maximum-ratio transmission (MRT) precoding, while S-APs simultaneously transmit sensing signals toward the sensing zones for target detection. The transmitted signals from C-APs and S-APs are respectively formulated as follows:

$$\mathbf{x}_m^c = \sum_{k=1}^K \sqrt{\rho \eta_{mk}^c} \hat{\mathbf{g}}_{mk} x_k^c, \quad (3)$$

$$\mathbf{x}_m^s = \sum_{l=1}^L \sqrt{\rho \eta_{ml}^s} \mathbf{a}_N(\theta_{ml}) x_l^s, \quad (4)$$

where ρ denotes the normalized transmit power and $\hat{\mathbf{g}}_{mk}$ is the MRT precoding vector. The data symbols x_k^c and sensing symbols x_l^s are assumed to be independent and normalized, i.e., $\mathbb{E}\{|x_k^c|^2\} = \mathbb{E}\{|x_l^s|^2\} = 1$. Furthermore, η_{mk}^c and η_{ml}^s represent the power allocation coefficients, which must satisfy the per-AP power constraint given by

$$a_m \mathbb{E}\{\|\mathbf{x}_m^c\|^2\} + (1-a_m) \mathbb{E}\{\|\mathbf{x}_m^s\|^2\} \leq \rho. \quad (5)$$

Accordingly, the corresponding received signal at the k -th UE can be expressed as

$$\begin{aligned} y_k &= \sum_{m=1}^M \mathbf{g}_{mk}^\dagger \mathbf{x}_m + n_k \\ &= \sum_{m=1}^M \sqrt{a_m \rho \eta_{mk}^c} \mathbf{g}_{mk}^\dagger \hat{\mathbf{g}}_{mk} x_k^c + n_k \\ &\quad + \sum_{k' \neq k} \sum_{m=1}^M \sqrt{a_m \rho \eta_{mk'}^c} \mathbf{g}_{mk'}^\dagger \hat{\mathbf{g}}_{mk'} x_{k'}^c \\ &\quad + \sum_{m=1}^M \sum_{l=1}^L \sqrt{(1-a_m) \rho \eta_{ml}^s} \mathbf{g}_{mk}^\dagger \mathbf{a}_N(\theta_{ml}) x_l^s, \end{aligned} \quad (6)$$

where n_k denotes additive white Gaussian noise (AWGN) with $n_k \sim \mathcal{CN}(0, 1)$. Since the APs lack instantaneous channel state information (CSI), the signal-to-interference-plus-noise ratio (SINR) of the k -th UE is derived using the *use-and-then-forget* bounding technique [12]. Accordingly, the SINR for the k -th UE can be expressed as

$$\text{SINR}_k = \frac{|\text{DS}_k|^2}{\mathbb{E}\{|\text{BU}_k|^2\} + \sum_{k' \neq k} \mathbb{E}\{|\text{IUI}_{kk'}|^2\} + \mathbb{E}\{|\text{IS}_k|^2\} + 1}, \quad (7)$$

where

$$\text{DS}_k \triangleq \mathbb{E} \left\{ \sum_{m=1}^M \sqrt{a_m \rho \eta_{mk}^c} \mathbf{g}_{mk}^\dagger \hat{\mathbf{g}}_{mk} \right\}, \quad (8a)$$

$$\text{BU}_k \triangleq \left(\sum_{m=1}^M \sqrt{a_m \rho \eta_{mk}^c} \mathbf{g}_{mk}^\dagger \hat{\mathbf{g}}_{mk} \right) - \text{DS}_k, \quad (8b)$$

$$\text{IUI}_{kk'} \triangleq \sum_{m=1}^M \sqrt{a_m \rho \eta_{mk'}^c} \mathbf{g}_{mk'}^\dagger \hat{\mathbf{g}}_{mk'}, \quad (8c)$$

$$\text{IS}_k \triangleq \sum_{m=1}^M \sum_{l=1}^L \sqrt{(1-a_m) \rho \eta_{ml}^s} \mathbf{g}_{mk}^\dagger \mathbf{a}_N(\theta_{ml}). \quad (8d)$$

These terms respectively represent the strength of the desired signal, the beamforming uncertainty due to imperfect CSI, inter-user interference, and interference from S-APs. The closed-form expression of (7) is provided in (9) at the top of the next page.

C. Eavesdropping and Sensing Operation

In this subsection, we focus on the sensing operation, which serves the dual purpose of target detection and physical-layer security enhancement. Concurrent with the downlink data transmission from C-APs, S-APs transmit dedicated sensing signals, as given in (4), toward the sensing zones. To quantify detection effectiveness, the sensing performance is evaluated using the MASR at the sensing-zone locations, defined as

$$\text{MASR}_l \triangleq \frac{P_{\text{DS}}^{\text{Sen}}(\theta_{ml})}{P_{\text{Com}}(\theta_{ml}) + P_{\text{DST}}^{\text{Sen}}(\theta_{ml})}, \quad (10)$$

$$\text{SINR}_k = \frac{\left(N \sum_{m=1}^M \sqrt{a_m \rho \eta_{mk}^c} \gamma_{mk} \right)^2}{N \sum_{k'=1}^K \sum_{m=1}^M a_m \rho \eta_{mk'}^c \beta_{mk'} \gamma_{mk'} + N \sum_{m=1}^M \sum_{l=1}^L (1 - a_m) \rho \eta_{ml}^s \beta_{mk} + 1} \quad (9)$$

$$\text{MASR}_l = \frac{N^2 \sum_{m=1}^M (1 - a_m) \eta_{ml}^s \zeta_{ml}}{N \sum_{k=1}^K \sum_{m=1}^M a_m \eta_{mk}^c \zeta_{ml} \gamma_{mk} + \sum_{m=1}^M \sum_{l' \neq l}^L (1 - a_m) \eta_{ml'}^s \zeta_{ml} |\mathbf{a}_N^\dagger(\theta_{ml}) \mathbf{a}_N(\theta_{ml'})|^2} \quad (12)$$

where

$$P^{\text{Com}}(\theta_{ml}) \triangleq \mathbb{E} \left\{ \left| \sum_{m=1}^M \sqrt{a_m} \mathbf{g}_{ml}^\dagger \mathbf{x}_m^c \right|^2 \right\}, \quad (11a)$$

$$P_{\text{DS}}^{\text{Sen}}(\theta_{ml}) \triangleq \mathbb{E} \left\{ \left| \sum_{m=1}^M \sqrt{(1 - a_m) \rho \eta_{ml}^s} \mathbf{g}_{ml}^\dagger \mathbf{a}_N(\theta_{ml}) x_l^s \right|^2 \right\}, \quad (11b)$$

$$P_{\text{DST}}^{\text{Sen}}(\theta_{ml}) \triangleq \mathbb{E} \left\{ \left| \sum_{l'=1}^L \sum_{m=1}^M \sqrt{(1 - a_m) \rho \eta_{ml'}^s} \mathbf{g}_{ml}^\dagger \mathbf{a}_N(\theta_{ml'}) x_{l'}^s \right|^2 \right\}. \quad (11c)$$

These respectively represent the communication power pattern, the desired sensing power pattern, and the distortion power pattern. Notably, the communication power pattern introduces distortion to the sensing operation, thereby degrading detection accuracy. The detailed expression of MASR_l is provided in (12) at the top of this page.

Meanwhile, multiple potential eavesdroppers are assumed to be located within the sensing zones, attempting to intercept confidential data transmitted by C-APs. The signal received by an eavesdropper at the l -th sensing zone is expressed as

$$y_l = \sum_{k=1}^K \sum_{m=1}^M \sqrt{a_m \rho \eta_{mk}^c} \mathbf{g}_{ml}^\dagger \hat{\mathbf{g}}_{mk} x_k^c + \sum_{m=1}^M \sum_{l'=1}^L \sqrt{(1 - a_m) \rho \eta_{ml'}^s} \mathbf{g}_{ml}^\dagger \mathbf{a}_N(\theta_{ml'}) x_{l'}^s + n_l, \quad (13)$$

where the first, second, and third terms correspond to the communication signals transmitted by C-APs, the sensing signals transmitted by S-APs, and AWGN, respectively. From the eavesdroppers' perspective, the communication signals act as desired signals, whereas the sensing signals function as intentionally introduced interference or artificial noise. Accordingly, the resulting SINR at the eavesdropper can be expressed as

$$\text{SINR}_l = \frac{\mathbb{E} \{ |\text{DS}_l|^2 \}}{\mathbb{E} \{ |\text{IS}_l|^2 \} + 1}, \quad (14)$$

where

$$\text{DS}_l \triangleq \sum_{k=1}^K \sum_{m=1}^M \sqrt{a_m \rho \eta_{mk}^c} \mathbf{g}_{ml}^\dagger \hat{\mathbf{g}}_{mk} \quad (15)$$

and

$$\text{IS}_l \triangleq \sum_{m=1}^M \sum_{l'=1}^L \sqrt{(1 - a_m) \rho \eta_{ml'}^s} \mathbf{g}_{ml}^\dagger \mathbf{a}_N(\theta_{ml'}) \quad (16)$$

represent the desired eavesdropping signal and the interference induced by sensing signals, respectively. The corresponding closed-form SINR expression is presented in (17)

at the top of the next page. While sensing signals act as interference to degrade eavesdropper reception, the overall security performance strongly depends on resource allocation. The key challenge, therefore, lies in the joint optimization of AP operational modes a_m and power allocation across communication and sensing links, as formulated in the following section.

III. JOINT POWER ALLOCATION

We formulate a resource allocation problem that encapsulates the inherent trade-offs among communication, sensing, and security. Increasing power allocation to C-APs improves communication performance but raises the risk of eavesdropping. In contrast, allocating power to S-APs enhances jamming and sensing performance at the expense of reduced data rates. To tackle this trade-off, we jointly optimize AP operational modes and power allocation using two complementary approaches: (i) maximizing the communication rate while adhering to security constraints, or (ii) minimizing the eavesdropping rate while satisfying quality of service (QoS) constraints. In both cases, a minimum sensing MASR threshold is imposed for all L sensing zones.

By invoking (2), the total transmit power at each AP is constrained by a maximum power budget, given by

$$N \sum_{k=1}^K a_m \eta_{mk}^c \gamma_{mk} + N \sum_{l=1}^L (1 - a_m) \eta_{ml}^s \leq 1. \quad (18)$$

A. Communication-Prioritized Optimization Method

This subsection presents the first optimization problem, which prioritizes communication performance by maximizing the worst-case UE SINR to ensure max-min fairness. For notational convenience, we first define $\mathbf{a} \triangleq \{a_1, \dots, a_M\}$, $\boldsymbol{\eta}^c \triangleq \{\eta_{m1}^c, \dots, \eta_{mK}^c\}$, and $\boldsymbol{\eta}^s \triangleq \{\eta_{m1}^s, \dots, \eta_{mL}^s\}$ for all m . The optimization problem is then formulated as

$$(\mathbf{P1}) : \max_{\mathbf{a}, \boldsymbol{\eta}^c, \boldsymbol{\eta}^s} \min_k \text{SINR}_k(\mathbf{a}, \boldsymbol{\eta}^c, \boldsymbol{\eta}^s) \quad (19a)$$

$$\text{s.t. } \text{SINR}_l(\mathbf{a}, \boldsymbol{\eta}^c, \boldsymbol{\eta}^s) \leq \nu, \forall l, \quad (19a)$$

$$\text{MASR}_l(\mathbf{a}, \boldsymbol{\eta}^c, \boldsymbol{\eta}^s) \geq \kappa, \forall l, \quad (19b)$$

$$N \sum_{k=1}^K \eta_{mk}^c \gamma_{mk} \leq a_m, \forall m, \quad (19c)$$

$$N \sum_{l=1}^L \eta_{ml}^s \leq 1 - a_m, \forall m, \quad (19d)$$

$$a_m \in \{0, 1\}, \forall m, \quad (19e)$$

where (19a) constrains the eavesdropper SINR, (19b) ensures the minimum sensing MASR, (19c) and (19d) impose the per-AP power constraints for C-APs and S-APs, and (19e) enforces binary AP selection.

$$\text{SINR}_l = \frac{N \sum_{k=1}^K \sum_{m=1}^M a_m \rho \eta_{mk}^c \zeta_{ml} \gamma_{mk}}{\sum_{m=1}^M \sum_{l'=1}^L (1 - a_m) \rho \eta_{ml'}^s \zeta_{ml} |\mathbf{a}_N^\dagger(\theta_{ml}) \mathbf{a}_N(\theta_{ml'})|^2 + 1} \quad (17)$$

First, we introduce a slack variable $t \triangleq \min_k \text{SINR}_k$. To address the integer binary constraint, the binary variables are relaxed. The constraint $a_m \in \{0, 1\}$ can be equivalently expressed as $a_m = a_m^2$. Meanwhile, the inequality $a_m^2 \leq a_m$ always holds for $a_m \in [0, 1]$. Following [13], a penalty term with parameter λ is added to drive a_m toward binary values, and a_m^2 is substituted in the power constraints for computational efficiency. The resulting non-convexity is then handled using the successive convex approximation (SCA) method. To reformulate the optimization problem, we apply the following inequality:

$$x^2 \geq x_0 (2x - x_0), \quad (20)$$

where x and x_0 are arbitrary real numbers.

Following the above transformations, the optimization problem is reformulated as

$$\begin{aligned} \text{(P2)} : \quad & \max_{\mathbf{a}, \boldsymbol{\eta}^c, \boldsymbol{\eta}^s, t} t - \lambda \sum_{m=1}^M a_m - a_m^{(n)} \left(2a_m - a_m^{(n)} \right) \\ \text{s.t.} \quad & \text{SINR}_k(\mathbf{a}, \boldsymbol{\eta}^c, \boldsymbol{\eta}^s) \geq t, \forall m, \quad (21a) \end{aligned}$$

$$\text{SINR}_l(\mathbf{a}, \boldsymbol{\eta}^c, \boldsymbol{\eta}^s) \leq \nu, \forall l, \quad (21b)$$

$$\text{MASR}_l(\mathbf{a}, \boldsymbol{\eta}^c, \boldsymbol{\eta}^s) \geq \kappa, \forall l, \quad (21c)$$

$$N \sum_{k=1}^K \eta_{mk}^c \gamma_{mk} \leq a_m^{(n)} \left(2a_m - a_m^{(n)} \right), \forall m, \quad (21d)$$

$$N \sum_{l=1}^L \eta_{ml}^s \leq (1 - a_m^2), \forall m, \quad (21e)$$

$$0 \leq a_m \leq 1, \forall m. \quad (21f)$$

where $(\cdot)^{(n)}$ denotes the feasible solution in the n -th iteration.

Having relaxed the binary variables and power constraints, the main challenge arises from the non-convexity of the constraints (21a)–(21c). This issue is addressed using SCA. Specifically, constraint (21a) is reformulated as

$$\begin{aligned} & \frac{\left(N \sum_{m=1}^M \sqrt{a_m \rho \eta_{mk}^c} \gamma_{mk} \right)^2}{t} \geq \rho \sum_{m=1}^M a_m \mu_{mk} \\ & + N \sum_{m=1}^M \sum_{l=1}^L \rho \eta_{ml}^s \beta_{mk} + 1, \quad (22) \end{aligned}$$

where

$$\mu_{mk} \triangleq N \sum_{k'=1}^K \eta_{mk'}^c \beta_{mk'} \gamma_{mk'} - N \sum_{l=1}^L \eta_{ml}^s \beta_{mk}. \quad (23)$$

Then, (22) can be reformulated as

$$\begin{aligned} & \frac{\left(2N \sum_{m=1}^M \sqrt{a_m \eta_{mk}^c} \gamma_{mk} \right)^2}{t} + \sum_{m=1}^M (a_m - \mu_{mk})^2 \geq \\ & \sum_{m=1}^M (a_m + \mu_{mk})^2 + 4N \sum_{m=1}^M \sum_{l=1}^L \eta_{ml}^s \beta_{mk} + 4/\rho. \quad (24) \end{aligned}$$

To obtain a concave lower bound for the left-hand side of the

above inequality, we apply the following relationship:

$$\frac{x^2}{y} \geq \frac{x_0}{y_0} \left(2x - \frac{x_0}{y_0} y \right), y > 0, \quad (25)$$

where y, y_0 denote arbitrary real numbers.

Using (20) and (25), (24) can be reformulated as

$$\begin{aligned} & q_k^{(n)} \left(4N \sum_{m=1}^M \sqrt{a_m \eta_{mk}^c} \gamma_{mk} - q_k^{(n)} t \right) + \\ & \sum_{m=1}^M \left(a_m^{(n)} - \mu_{mk}^{(n)} \right) \left(2(a_m - \mu_{mk}) - \left(a_m^{(n)} - \mu_{mk}^{(n)} \right) \right) \geq \\ & \sum_{m=1}^M (a_m + \mu_{mk})^2 + 4N \sum_{m=1}^M \sum_{l=1}^L \eta_{ml}^s \beta_{mk} + 4/\rho, \quad (26) \end{aligned}$$

where

$$q_k^{(n)} \triangleq \frac{2N \sum_{m=1}^M \sqrt{a_m^{(n)} (\eta_{mk}^c)^{(n)} \gamma_{mk}}}{t^{(n)}}. \quad (27)$$

Following the same procedure and invoking (20), we recast (21b) and (21c) as

$$\begin{aligned} & \sum_{m=1}^M \left(a_m^{(n)} - \varrho_{ml}^{(n)} \right) \left(2(a_m - \varrho_{ml}) - \left(a_m^{(n)} - \varrho_{ml}^{(n)} \right) \right) \\ & + 4\nu \sum_{m=1}^M \sum_{l'=1}^L \eta_{ml'}^s \zeta_{ml} |\mathbf{a}_N^\dagger(\theta_{ml}) \mathbf{a}_N(\theta_{ml'})|^2 + \frac{4\nu}{\rho} \\ & \geq \sum_{m=1}^M (a_m + \varrho_{ml})^2, \quad (28) \end{aligned}$$

and

$$\begin{aligned} & 4N^2 \sum_{m=1}^M \eta_{ml}^s \zeta_{ml} + \sum_{m=1}^M \left(a_m^{(n)} - \omega_{ml}^{(n)} \right) \\ & \times \left(2(a_m - \omega_{ml}) - \left(a_m^{(n)} - \omega_{ml}^{(n)} \right) \right) \geq \\ & 4\kappa \sum_{l' \neq l}^L \eta_{ml'}^s \zeta_{ml} |\mathbf{a}_N^\dagger(\theta_{ml}) \mathbf{a}_N(\theta_{ml'})|^2 \\ & + \sum_{m=1}^M (a_m + \omega_{ml})^2, \quad (29) \end{aligned}$$

where

$$\begin{aligned} \varrho_{ml} & \triangleq N \sum_{k=1}^K \eta_{mk}^c \zeta_{ml} \gamma_{mk} \\ & + \nu \sum_{l'=1}^L \eta_{ml'}^s \zeta_{ml} |\mathbf{a}_N^\dagger(\theta_{ml}) \mathbf{a}_N(\theta_{ml'})|^2, \quad (30) \end{aligned}$$

$$\begin{aligned} \omega_{ml} & \triangleq N^2 \eta_{ml}^s \zeta_{ml} + \kappa \sum_{k=1}^K N \eta_{mk}^c \zeta_{ml} \gamma_{mk} \\ & - \kappa \sum_{l' \neq l}^L \eta_{ml'}^s \zeta_{ml} |\mathbf{a}_N^\dagger(\theta_{ml}) \mathbf{a}_N(\theta_{ml'})|^2. \quad (31) \end{aligned}$$

Substituting the non-convex constraints with their convex approximations transforms the problem into a standard convex program, given by

$$\begin{aligned} \text{(P3)} : \quad & \max_{\mathbf{a}, \boldsymbol{\eta}^c, \boldsymbol{\eta}^s, t} t - \lambda \sum_{m=1}^M a_m - a_m^{(n)} \left(2a_m - a_m^{(n)} \right) \\ \text{s.t.} \quad & (26), (28), (29), (21d), (21e), (21f). \end{aligned}$$

This reformulated problem adheres to convex optimization theory and can be efficiently solved using standard solvers such as CVX. The iterative procedure starts from a randomly generated feasible point $\tilde{\mathbf{x}} \triangleq \{\mathbf{a}, \boldsymbol{\eta}^c, \boldsymbol{\eta}^s\}$ and updates the solution iteratively. The obtained solution $\tilde{\mathbf{x}}^*$ is then used as the initial point for the next iteration, and the process continues until convergence.

B. Security-Prioritized Optimization Method

The second optimization strategy prioritizes security by minimizing the maximum eavesdropper SINR while maintaining minimum SINR thresholds for UEs. This formulation inverts the objective-constraint relationship of Problem (P1), where communication performance is treated as constraint rather than an objective. By applying the same relaxation technique as in Problem (P1), the optimization problem is formulated as

$$\begin{aligned} \text{(P4)} : \quad & \min_{\mathbf{a}, \boldsymbol{\eta}^c, \boldsymbol{\eta}^s, t} \quad t + \lambda \sum_{m=1}^M a_m - a_m^{(n)} \left(2a_m - a_m^{(n)} \right) \\ \text{s.t.} \quad & \text{SINR}_l(\mathbf{a}, \boldsymbol{\eta}^c, \boldsymbol{\eta}^s) \leq t, \forall l, \quad (32a) \\ & \text{SINR}_k(\mathbf{a}, \boldsymbol{\eta}^c, \boldsymbol{\eta}^s) \geq \varsigma, \forall l, \quad (32b) \\ & (21c), (21d), (21e), (21f). \end{aligned}$$

The sensing performance constraint is treated in the same manner as in the communication-prioritized optimization method; hence, the detailed derivation is omitted for brevity. We now address the non-convex constraints (32a) and (32b). Specifically, constraint (32a) is reformulated as

$$\begin{aligned} & \sum_{m=1}^M (t + \varepsilon_{ml})^2 + \sum_{m=1}^M (a_m - \delta_{ml})^2 + 4t/\rho \\ & \geq \sum_{m=1}^M (t - \varepsilon_{ml})^2 + \sum_{m=1}^M (a_m + \delta_{ml})^2 \quad (33) \\ & + 4f_{ml}(t, a_m, \varepsilon_{ml}) \end{aligned}$$

where

$$\delta_{ml} = N \sum_{k=1}^K \eta_{mk}^c \zeta_{ml} \gamma_{mk}, \quad (34a)$$

$$\varepsilon_{ml} = \sum_{l'=1}^L \eta_{ml'}^s \zeta_{ml} |\mathbf{a}_N^\dagger(\theta_{ml}) \mathbf{a}_N(\theta_{ml'})|^2, \quad (34b)$$

$$f_{ml}(t, a_m, \varepsilon_{ml}) = t \sum_{m=1}^M a_m \varepsilon_{ml}. \quad (34c)$$

For the non-convex function $f_{ml}(t, a_m, \varepsilon_{ml})$, we form a convex approximation by applying a first-order Taylor expansion as

$$\begin{aligned} f_{ml}^{(n)}(t, a_m, \varepsilon_{ml}) = & \sum_{m=1}^M \left(a_m^{(n)} \varepsilon_{ml}^{(n)} t + a_m^{(n)} t^{(n)} \varepsilon_{ml} \right. \\ & \left. + \varepsilon_{ml}^{(n)} t^{(n)} a_m - 2a_m^{(n)} \varepsilon_{ml}^{(n)} t^{(n)} \right). \quad (35) \end{aligned}$$

By invoking (20) and (35), we obtain a concave lower bound of the left-hand side, as follows:

$$\begin{aligned} & \sum_{m=1}^M \left(t^{(n)} + \varepsilon_{ml}^{(n)} \right) \left(2(t + \varepsilon_{ml}) - \left(t^{(n)} + \varepsilon_{ml}^{(n)} \right) \right) \\ & + \sum_{m=1}^M \left(a_m^{(n)} - \delta_{ml}^{(n)} \right) \left(2(a_m - \delta_{ml}) - \left(a_m^{(n)} - \delta_{ml}^{(n)} \right) \right) \\ & + 4t/\rho \geq \sum_{m=1}^M (a_m + \delta_{ml})^2 + \sum_{m=1}^M (t - \varepsilon_{ml})^2 \\ & + 4f_{ml}^{(n)}(t, a_m, \varepsilon_{ml}). \quad (36) \end{aligned}$$

The communication quality constraint (32b) is reformulated using the same methodology as applied to constraint (21a), as

$$\begin{aligned} & \frac{\left(2N \sum_{m=1}^M \sqrt{a_m \eta_{mk}^c} \gamma_{mk} \right)^2}{\varsigma} + \sum_{m=1}^M (a_m - \mu_{mk})^2 \geq \\ & \sum_{m=1}^M (a_m + \mu_{mk})^2 + 4N \sum_{m=1}^M \sum_{l=1}^L \eta_{ml}^s \beta_{mk} + 4/\rho. \quad (37) \end{aligned}$$

In contrast, (20) is applied to obtain a concave lower bound for the left-hand side, yielding the constraint as

$$\begin{aligned} & \frac{2N \sum_{m=1}^M \sqrt{a_m^{(n)} (\eta_{mk}^c)^{(n)} \gamma_{mk}}}{\varsigma} \left(4N \sum_{m=1}^M \sqrt{a_m \eta_{mk}^c} \gamma_{mk} \right. \\ & \left. - 2N \sum_{m=1}^M \sqrt{a_m^{(n)} (\eta_{mk}^c)^{(n)} \gamma_{mk}} \right) + \\ & \sum_{m=1}^M \left(a_m^{(n)} - \mu_{mk}^{(n)} \right) \left(2(a_m - \mu_{mk}) - \left(a_m^{(n)} - \mu_{mk}^{(n)} \right) \right) \geq \\ & \sum_{m=1}^M (a_m + \mu_{mk})^2 + 4N \sum_{m=1}^M \sum_{l=1}^L \eta_{ml}^s \beta_{mk} + 4/\rho. \quad (38) \end{aligned}$$

Based on the convex approximations, the reformulated optimization problem is presented as

$$\begin{aligned} \text{(P5)} : \quad & \min_{\mathbf{a}, \boldsymbol{\eta}^c, \boldsymbol{\eta}^s, t} \quad t + \lambda \sum_{m=1}^M a_m - a_m^{(n)} \left(2a_m - a_m^{(n)} \right) \\ \text{s.t.} \quad & (36), (38), (29), (21d), (21e), (21f). \end{aligned}$$

Similar to the communication-prioritized optimization problem, this convex program can be efficiently solved using CVX within the SCA framework.

IV. NUMERICAL SIMULATIONS

This section presents numerical results validating the proposed optimization frameworks and evaluating their performance. We consider a 500×500 m² area where M APs and K UEs are uniformly distributed, and L sensing zones are randomly placed. Each AP is assumed to possess prior knowledge of the angular directions to all sensing zones for target detection. The system parameters are set to $(M, N, L) = (32, 8, 2)$, $\nu = 0.5$, $\varsigma = 4$ dB, and $\kappa = 2$ dB. The network parameters are set to $\tau = 200$ and $\tau_t = K + L$. The transmit powers for data and pilot signals are set to $\rho = 1$ W and $\rho_t = 0.25$ W, respectively.

Fig. 2 illustrates the trade-off between the two proposed optimization strategies: communication-prioritized (CP) and security-prioritized (SP). Each strategy excels in its primary objective. The SP strategy lowers the eavesdropping rate by allocating more power to sensing signals, which makes the eavesdropper's channel worse but also lowers the communication rate. Conversely, the CP strategy maintains a higher communication rate by prioritizing C-AP resource allocation, benefiting UEs but leading to an increased eavesdropping rate due to lower sensing power. Overall, the CP attains a higher secrecy rate, as excessive power allocation to sensing yields diminishing security gains.

Fig. 3 examines the impact of the minimum sensing requirement κ on the secrecy rate performance for both opti-

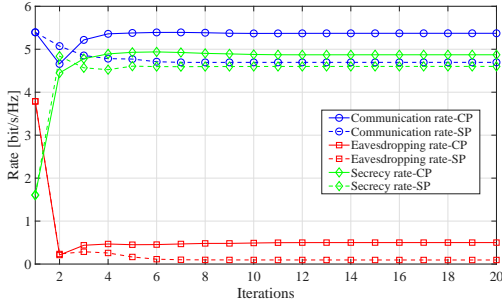


Fig. 2. Convergence of communication, eavesdropping, and secrecy rates.

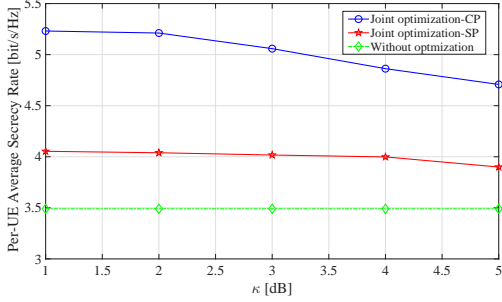


Fig. 3. Comparison of per-UE average secrecy rate under different κ .

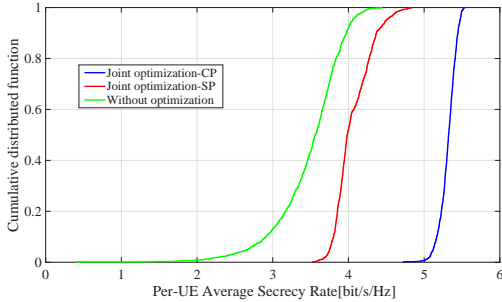


Fig. 4. CDF of the per-UE average secrecy rate.

mization strategies, using an average power allocation scheme used as a baseline. The CP strategy significantly enhances secrecy rates by primarily allocating power to communication links, while ensuring minimal power is dedicated to sensing to fulfill the requirement. However, as κ increases, the CP strategy suffers severe performance degradation since more power must be redirected from communication to sensing, reducing user rates and consequently secrecy performance. Conversely, the SP strategy maintains robust performance under increasing κ . The inherent allocation of substantial power to sensing facilitates eavesdropper suppression, allowing higher sensing demands to be met without significant power redistribution, thereby ensuring stable secrecy rate performance across the parameter range.

Fig. 4 presents the cumulative distribution function (CDF) of secrecy rates for both optimization strategies, benchmarked against the average power allocation scheme. The CP strategy consistently outperforms the others, achieving higher secrecy at all probability levels. Specifically, it attains a median secrecy rate of 5.1 bit/s/Hz, substantially exceeding that of the SP method. Although the SP strategy yields lower secrecy

rates than the CP strategy, it still provides considerable improvement over the baseline, maintaining secrecy rates above 3.5 bit/s/Hz and demonstrating robust security performance.

V. CONCLUSION

This paper investigated a multi-static CF-mMIMO ISAC system employing AP selection. Through closed-form derivations of the communication rate, eavesdropping rate, and MASR, we quantified the interplay between communication and sensing functions while demonstrating the security benefits of AP selection. Optimization problems were proposed to maximize communication rates or minimize eavesdropping rates under sensing performance and power budget constraints. Numerical results validated the theoretical analysis and confirmed the effectiveness of the proposed power allocation framework.

ACKNOWLEDGEMENT

This work was supported in part by JST, CRONOS, Japan Grant Number JPMJCS24N1, and in part by MIC/FORWARD under Grant JPMI240710001.

REFERENCES

- [1] D. Xu, X. Yu, D. W. K. Ng, A. Schmeink, and R. Schober, "Robust and secure resource allocation for ISAC systems: A novel optimization framework for variable-length snapshots," *IEEE Trans. Commun.*, vol. 70, no. 12, pp. 8196–8214, 2022.
- [2] R. Yang, C.-X. Wang, J. Huang, E.-H. M. Aggoune, and Y. Hao, "A novel 6G ISAC channel model combining forward and backward scattering," *IEEE Trans. Wireless Commun.*, vol. 22, no. 11, pp. 8050–8065, 2023.
- [3] Y. Fang, L. Qiu, X. Liang, and C. Ren, "Cell-free massive MIMO systems with oscillator phase noise: Performance analysis and power control," *IEEE Trans. Veh. Technol.*, vol. 70, no. 10, pp. 10048–10064, 2021.
- [4] F. Liu, Y. Cui, C. Masouros, J. Xu, T. X. Han, Y. C. Eldar, and S. Buzzi, "Integrated sensing and communications: Toward dual-functional wireless networks for 6G and beyond," *IEEE J. Sel. Areas Commun.*, vol. 40, no. 6, pp. 1728–1767, 2022.
- [5] Z. Wei, F. Liu, C. Masouros, N. Su, and A. P. Petropulu, "Toward multi-functional 6G wireless networks: Integrating sensing, communication, and security," *IEEE Commun. Magazine*, vol. 60, no. 4, pp. 65–71, 2022.
- [6] T. Matsumine, H. Ochiai, and J. Shikata, "Physical layer security for integrated sensing and communication: A survey," *IEEE Open J. Commun. Soc.*, vol. 6, pp. 6690–6743, 2025.
- [7] S. Rivetti, E. Björnson, and M. Skoglund, "Secure spatial signal design for ISAC in a cell-free MIMO network," in *Proc. 2024 IEEE Wireless Commun. and Netw. Conf. (WCNC)*. IEEE, 2024, pp. 01–06.
- [8] Z. Ren, J. Xu, L. Qiu, and D. Wing Kwan Ng, "Secure cell-free integrated sensing and communication in the presence of information and sensing eavesdroppers," *IEEE J. Sel. Areas Commun.*, vol. 42, no. 11, pp. 3217–3231, 2024.
- [9] S. Kim and S. Jeon, "Fronthaul compression and beamforming optimization for secure cell-free ISAC systems," *IEEE Wireless Commun. Lett.*, pp. 1–1, 2025.
- [10] M. Elfiatoure, M. Mohammadi, H. Quoc Ngo, H. Shin, and M. Matthaiou, "Multiple-target detection in cell-free massive MIMO-assisted ISAC," *IEEE Trans. Wireless Commun.*, vol. 24, no. 5, pp. 4283–4298, 2025.
- [11] H. Q. Ngo, A. Ashikhmin, H. Yang, E. G. Larsson, and T. L. Marzetta, "Cell-free massive MIMO versus small cells," *IEEE Trans. Wireless Commun.*, vol. 16, no. 3, pp. 1834–1850, 2017.
- [12] N. Li and P. Fan, "Impact of UE hardware impairments on uplink spectral efficiency of cell-free massive MIMO network," in *Proc. 2023 IEEE Wireless Commun. and Netw. Conf. (WCNC)*, 2023, pp. 1–6.
- [13] E. Che, H. D. Tuan, and H. H. Nguyen, "Joint optimization of cooperative beamforming and relay assignment in multi-user wireless relay networks," *IEEE Trans. Wireless Commun.*, vol. 13, no. 10, pp. 5481–5495, 2014.